Real-Time Wind Velocity Monitoring Based on Acoustic Tomography

Yong Bao and Jiabin Jia

Abstract Wind-related disasters cause tremendous loss around the world, therefore a fast, low-cost but accurate wind velocity monitoring technique is highly desirable and will provide great benefits for wind risk management. Acoustic travel-time tomography, which utilise the dependence of sound speed on the wind velocity along the sound propagation path, is considered to be a promising remote sensing technique for wind velocity monitoring. The success of acoustic tomography technique stems from then various advantage of non-invasive, low cost and easy to implement when compared to other techniques. This chapter describes the fundamentals of the simultaneously multi-channel time-of-flight measurements and the tomographic reconstruction of 2D horizontal wind velocity distributions based on the use of offline iteration method. The feasibility and effectiveness of the proposed methods will be numerically validated in a simulation study.

Keywords Acoustic tomography · Wind velocity · Remote sensing

1 Introduction

Extreme strong wind is dangerous for people and cause significant damage to buildings, infrastructures, agricultural, forestry and property with the damage being highly unpredictable. There are many aspects to be looked into by researchers and engineers [1, 2]. One of the issues is accurate and reliable measurement of wind velocity, particularly in the atmospheric boundary layer, which is the lower part of the atmosphere. A fast, low-cost but accurate wind velocity monitoring technique is highly desirable and will provide great benefits in order to reduce wind-related disasters for safer and securer communities.

Y. Bao · J. Jia (✉)
School of Engineering, Institute for Digital Communications,
The University of Edinburgh, Edinburgh, UK
e-mail: jiabin.jia@ed.ac.uk

T. S. Durrani et al. (eds.), *Geological Disaster Monitoring Based on Sensor Networks*, Springer Natural Hazards, https://doi.org/10.1007/978-981-13-0992-2_9

There are a number of efforts in developing robust and accurate wind velocity measurement techniques. Conventional cup anemometer is the most used device but they have the drawbacks including intrusive, single-point sensing and corrosion in the harsh environment [3]. SODAR (SOund Detection And Ranging) and LIDAR (LIght Detection And Ranging), the two remote sensing technique both employ the Doppler effect to acquire wind observations, are very expensive and relatively power hungry [4]. Compared to other techniques, acoustic tomography is one of few that can deliver accurate quantitative reconstruction of the whole temperature field with lower equipment cost.

Early application of acoustic tomography was firstly proposed in 1990 by Spiesberger [5] and first experimental implementation was completed in 1994 by Wilson and Thomson [6]. Their tomography array consisted of 3 transmitters and 5 receivers to cover a rectangular area of 200 m by 200 m with 50 m resolution. Later, similar acoustic tomography system has been completed in the University of Leipzig, Germany. In serval experiments since 1996 [7–9], the size and number of transducers of the acoustic tomography system were variable, from 100 m by 200 m with 20 m resolution to 200 m by 240 m with 50 m resolution. A first 3D array for acoustic tomography was built at the Boulder Atmospheric Observatory [10]. 9 transmitters and 15 receivers were placed around the square sensing area, with the side length of 80 m, at three adjustable height.

The tomographic reconstruction of the wind velocity is generally difficult. The inverse problem is under-determined due to the limited number of measurements. Therefore, the solution is not unique. Besides, the travel-time measurement is line integral of the wind velocity distribution, which results in an ill-posed inverse problem. This means that the reconstruction results are very sensitive to the measurement noise. Numerous algorithms have been developed to solve the acoustic tomographic inverse problem. These algorithms can be categorised into three main branches including algebraic-based algorithms [8, 11, 12], sparse reconstruction framework [13–15] and stochastic-based algorithms [6, 7, 16–18].

This chapter describes the fundamentals of the measurement method and the tomographic reconstruction of 2D horizontal wind velocity distributions. Section 2.1 reviews the forward modelling of acoustic travel-time tomography. Then in Sect. 2.2 and 2.3 the Time-Of-Flight (TOF) data collection and vector tomography reconstruction algorithm is illustrated. Numerical simulation results are discussed in Sect. 3 and the conclusion is drawn in Sect. 4.

2 Methodology

2.1 Forward Modelling of Acoustic Tomography

Acoustic travel-time tomography mainly utilises the strong dependence of sound propagation on the spatial distribution of air temperature and velocity. A typical

setup for acoustic travel-time tomography is illustrated in Fig. 1. The whole square sensing area is surrounded by 16 acoustic transceivers. The time-of-flight (TOF) between each transducer pairs are recorded along 96 ray paths. Given the position of the transceivers and the TOF measurements, the corresponding wind velocity field can be recovered. The acoustic transducer array covers a sensing area of 100 m by 100 m with 5 m resolution, therefore the reconstructed image is a vector field with 20 by 20 pixels.

The wavelength of the acoustic signal is much smaller than the medium inhomogeneities in size, therefore, geometric acoustics model is used and the acoustic signals are considered to propagate along sound ray paths between transducer pairs.

According to the geometrical acoustic assumption, the group velocity $\boldsymbol{u}$ (the observable quantity using acoustic tomography technique) of a sound wave in air is defined as [19]:

$$\boldsymbol{u} = c_L \boldsymbol{n} + \boldsymbol{v} \tag{1}$$

where c_L denotes the Laplace's sound speed which only depends on air temperature, $\boldsymbol{v}$ represents the wind velocity and $\boldsymbol{n}$ is the direction normal to the wave front.

With the use of acoustic transducer array placed around the sensing area, the group velocity is determined according to the time-of-flight (TOF) measurements, which is defined as:

$$\mathrm{T} = \int_{\Gamma} \frac{d\boldsymbol{s}}{(c_L \boldsymbol{n} + \boldsymbol{v})} \tag{2}$$

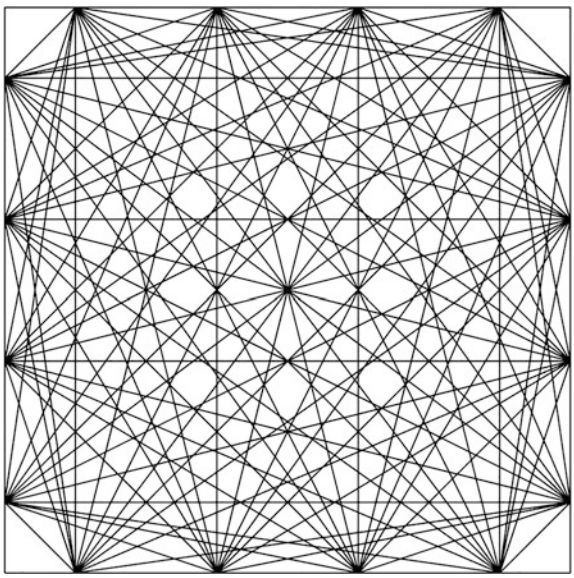

Fig. 1 Acoustic tomography problem setup

where τ is the TOF along ray path Γ and $\boldsymbol{s}$ is the unit direction vector along the ray path.

Equation (2) can be linearized as:

$$\begin{aligned}\tau &= \int_{\Gamma} \frac{d\boldsymbol{s}}{(c_{L0}+\boldsymbol{\Delta} c_L)\boldsymbol{n}+\boldsymbol{v}} \\ &= \int_{\Gamma} \frac{(c_{L0}\boldsymbol{n}-(\boldsymbol{\Delta} c_L\boldsymbol{n}+\boldsymbol{v}))d\boldsymbol{s}}{(c_{L0}\boldsymbol{n})^2-(\boldsymbol{\Delta} c_L\boldsymbol{n}+\boldsymbol{v})^2} \\ &\approx \int_{\Gamma} \frac{d\boldsymbol{s}}{c_{L0}\boldsymbol{n}} - \int_{\Gamma} \frac{(\boldsymbol{\Delta} c_L\boldsymbol{n}+\boldsymbol{v})d\boldsymbol{s}}{(c_{L0}\boldsymbol{n})^2} \\ &= \tau_0 - \frac{1}{c_{L0}^2}\int_{\Gamma} (\boldsymbol{\Delta} c_L\boldsymbol{n}+\boldsymbol{v})d\boldsymbol{s}\end{aligned} \tag{3}$$

where c_{L0} represents the average Laplace's sound speed and $\boldsymbol{\Delta} c_L = c_L - c_{L0}$ is the group velocity perturbations caused by temperature, and $\boldsymbol{v}$ is the wind velocity. Typically, the group velocity perturbation $\boldsymbol{\Delta u} = \boldsymbol{\Delta} c_L\boldsymbol{n}+\boldsymbol{v}$ is much smaller than c_{L0}, hence Eq. (3) can be rearranged so that TOF perturbations are linearly related with the $\boldsymbol{\Delta u}$.

$$(\tau_0-\tau)c_{L0}^2 = \int_{\Gamma} (\boldsymbol{\Delta} c_L\boldsymbol{n}+\boldsymbol{v})d\boldsymbol{s} = \int_{\Gamma} \boldsymbol{\Delta u}\, d\boldsymbol{s} \tag{4}$$

Because the acoustic refraction effect is usually ignored in this type of application, the ray path is considered as a straight line from the transmitter to the receiver [11]. For any point along the line, $\boldsymbol{s}$ is a constant vector determined by the sensor placement and $\boldsymbol{n}\cdot\boldsymbol{s} = 1$. Based on this straight line assumption, reciprocal tomography is employed in acoustic tomography system. The group velocity perturbations in one direction is given by $\boldsymbol{\Delta u}_+ = \boldsymbol{\Delta} c_L\boldsymbol{n} - \boldsymbol{v}$, while in the opposite direction $\boldsymbol{\Delta u}_- = \boldsymbol{\Delta} c_L\boldsymbol{n}+\boldsymbol{v}$. Therefore the influence brought by $\boldsymbol{\Delta} c_L\boldsymbol{n}$ and $\boldsymbol{v}$ is separated using the back and forth TOF measurements τ_+ and τ_- in two opposite directions (Fig. 2).

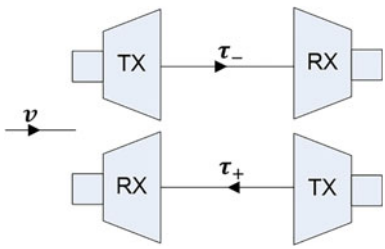

Fig. 2 Reciprocal transmission

$$l_\Gamma = \frac{(\tau_+ - \tau_-)c_{L0}^2}{2} = \int_\Gamma \boldsymbol{v}d\boldsymbol{s} \tag{5}$$

Then Eq. (5) can be discretized as:

$$\begin{bmatrix} lx_{\Gamma,\mathrm{i}} \\ ly_{\Gamma,\mathrm{i}} \end{bmatrix} = \begin{bmatrix} \sum_{j=1}^{N} v_{x_j} s_{i,j} \cos(\theta) \\ \sum_{j=1}^{N} v_{y_j} s_{i,j} \sin(\theta) \end{bmatrix} \tag{6}$$

where v_{x_j} and v_{y_j} are the directional wind velocity in j-th pixel, $s_{i,j}$ is the segment length for each ray path cover across one pixel, and $[\cos\theta, \sin\theta]$ is the direction vector from the transmitter to the receiver. Equation (6) can be written in a matrix form:

$$\boldsymbol{L_\Gamma} = \boldsymbol{SV} \tag{7}$$

where $\boldsymbol{L_\Gamma} \in \mathbb{R}^{2N}$ and N is the number of ray path, $\boldsymbol{V} = [\boldsymbol{V_x}; \boldsymbol{V_y}]$, $\boldsymbol{V_x}, \boldsymbol{V_y} \in \mathbb{R}^M$, M is the number of pixels; $\boldsymbol{S} = [\boldsymbol{S_x}; \boldsymbol{S_y}]$, and $\boldsymbol{S_x}, \boldsymbol{S_y} \in \mathbb{R}^{N*M}$ are the directional ray length matrix whose elements are $s_{i,j}\cos(\theta)$ and $s_{i,j}\sin(\theta)$ respectively.

2.2 Acoustic Signal Process for TOF Detection

In conventional acoustic tomography system, each transmitter is sequentially switched on to transmit acoustic signals to the different receivers. That approach has small interference for TOF detection as acoustic signals from different transmitters are separated in a different time slot at the receiver. However, the temporal resolution of the system is limited and it may not be able to capture the dynamic wind velocity changes in the sensing area. In order to improve the temporal resolution of acoustic tomography system, all the acoustic transceivers could transmit and receive acoustic signals simultaneously. As a result, the measurement time is significantly reduced compared with the pairwise sequential measurement strategy. In this operation, each received signal is a summation of all P delayed source signals.

$$y_j(t) = \sum_{i=1}^{\mathrm{P}} x_i\left(t - \Delta t_{i,j}\right) + n_j(t), \quad \mathrm{i} \neq \mathrm{j} \tag{8}$$

where $y_j(t)$ refers to the received signal at j-th receiver, $x_i(t)$ is the source signal from i-th transmitter and $\Delta t_{i,j}$ represents their corresponding delay time, which is the TOF in i-th ray path. $n_j(t)$ is the local noise received at j-th receiver.

The summed signals must be separated at the receiver side first, then their individual delay time $\Delta t_{i,j}$ can be estimated based on the cross-correlation detection defined as below.

$$R_{y_j x_k}(l) = \sum_{l=-\infty}^{+\infty} \left[y_j(t) x_k(t-l) \right] = \sum_{l=-\infty}^{+\infty} \left[\left[\sum_{i=1, i\neq j}^{K} x_i\left(t - \Delta t_{i,j}\right) + n_j(t) \right] x_k(t-l) \right]$$
$$= \sum_{i=1, i\neq j, i\neq \mathrm{k}}^{\mathrm{P}} R_{x_i x_k}\left(l - \Delta t_{i,j}\right) + R_{x_k x_k}\left(l - \Delta t_{k,j}\right) + R_{n_j x_k}(l) \tag{9}$$

where l denotes the correlation delay and noise term $n_j(t)$ is uncorrelated with the source signal x_i, and x_k is the k-th reference signal waveform for cross-correlation detection.

In order to minimise the interference term $\sum_{i=1, i\neq j, i\neq \mathrm{k}}^{\mathrm{P}} R_{x_i x_k}\left(l - \Delta t_{i,j}\right)$ and noise term $R_{n_j x_k}(l)$, all the source signal waveforms should have good correlation property, such as sharp auto-correlation peak, but low cross-correlation value, for arbitrarily random delay $\Delta t_{i,j}$ and uncorrelated to the noise at the receiver.

Maximum Length Sequence (MLS) has a good asynchronous orthogonal property, which could be used to separate different source signals with arbitrary delay at the receiver [11]. However, when a large number of simultaneous acoustic sources are used, like 16 in this case, the cross-correlation property of MLS is relatively poor. Selecting and combining the preferred pairs of MLS together can improve cross-correlation property, like the Kasami sequence. In fact, the Kasami sequence has near optimal cross-correlation values close to the Welch lower bound [20].

Therefore, the Kasami sequence shown in Fig. 3 is selected to generate acoustic signals for simultaneous source signal transmission and separation. However, it is difficult to practically generate and transmit the Kasami sequence with the acoustic transceivers, because the spectrum of the Kasami sequence is arbitrarily wide with sharp edges and discontinuity in the time domain, but the acoustic transceiver is restricted to a limited bandwidth around a certain frequency. Therefore, before transmission, it is essential to modulate the Kasami sequence with a fixed carrier frequency, then a band-pass filter is applied to smooth the Kasami sequence and control its bandwidth.

As shown in Fig. 4, compared with the original Kasami sequence, the modulated and filtered Kasami sequence has a narrower bandwidth to meet the bandwidth specification for the acoustic transceivers.

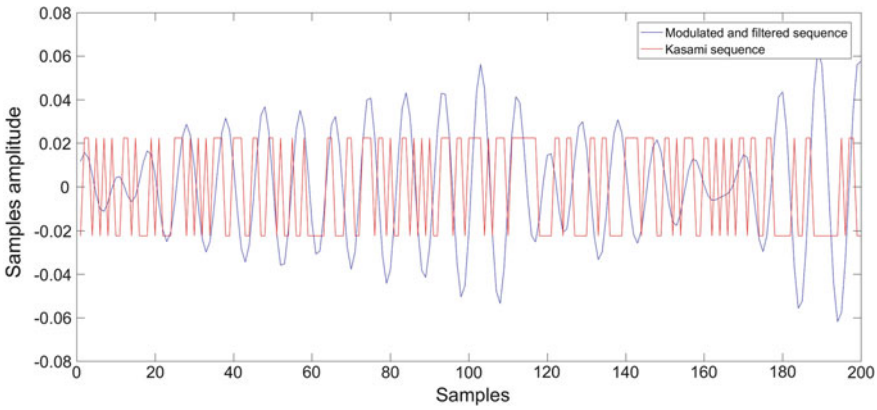

Fig. 3 Kasami sequence (red) and the output signal (blue) in time domain after modulation and band-pass filter (Color figure online)

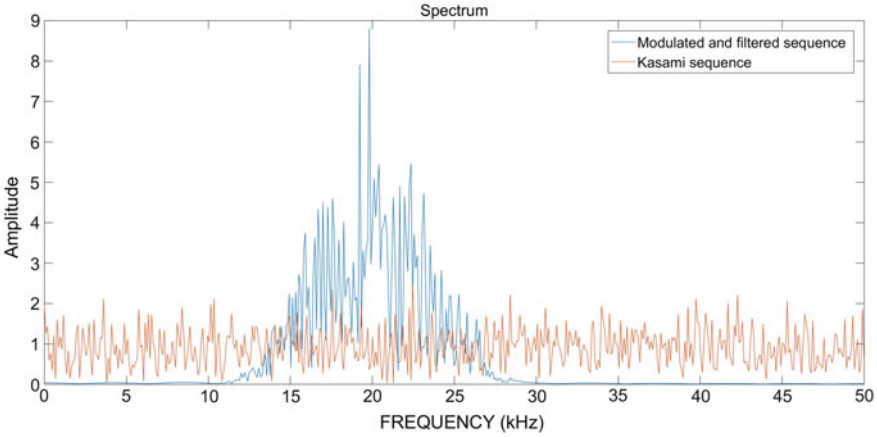

Fig. 4 Kasami sequence (red) and modulated and filtered output sequence (blue) in frequency domain. After modulation and band-pass filter, the bandwidth of output signal is limited and centred at the 20 kHz carrier frequency (Color figure online)

2.3 Wind Velocity Reconstruction

Tomographic reconstruction of wind velocity is considered as a typical vector field tomography problem, which recovers the wind velocity field from its line integrals calculated from reciprocal transmission TOF measurements.

Based on Helmholtz's theorem, a bounded wind velocity field $\boldsymbol{v}$ can be uniquely decomposed into three components.

$$\boldsymbol{v} = \boldsymbol{v}_S + \boldsymbol{v}_I + \boldsymbol{v}_H \tag{10}$$

where $\boldsymbol{v}_S(\nabla \cdot \boldsymbol{v}_S = 0)$ is the pure solenoidal component $(\nabla \cdot \boldsymbol{v}_S = 0)$, $\boldsymbol{v_I}(\nabla \times \boldsymbol{v_I} = 0)$ is the pure irrotational component, and $\boldsymbol{v_H}(\nabla \cdot \boldsymbol{v_H} = 0, \nabla \times \boldsymbol{v_H} = 0)$ is the harmonic component. However, according to theoretical analysis of vector tomography [21], it has been proved that the TOF measurements are not sufficient to fully reconstruct the whole vector field, only the divergence-free component $\boldsymbol{v}_S$ and $\boldsymbol{v_H}$ can be uniquely recovered from the line integrals. A brief description is presented as below.

Apply Eqs. (10) to (5) and use the potential function representation $\boldsymbol{v_I} = \nabla\phi$ and $\boldsymbol{v}_S = \nabla \times \psi$, the forward equation become:

$$\begin{aligned} l_\Gamma &= \int_{s_t}^{s_r} \boldsymbol{v_I} + \boldsymbol{v_S} + \boldsymbol{v_H}\, ds \\ &= \int_{s_t}^{s_r} \left[\left(\frac{\partial\phi}{\partial x}, \frac{\partial\phi}{\partial y} \right) + \left(\frac{\partial\psi}{\partial y}, -\frac{\partial\psi}{\partial x} \right) + \left(v_{H_x}, v_{H_y} \right) \right] \cdot (\cos\theta\, dx, \sin\theta\, dy) \\ &= \phi(sx_r, sy_r) - \phi(sx_t, sy_t) + \int_{sx_t}^{sx_r} \left(\frac{\partial\psi}{\partial y} + v_{H_x} \right) \cos\theta\, dx + \int_{sy_t}^{sy_r} \left(-\frac{\partial\psi}{\partial x} + v_{H_y} \right) \sin\theta\, dy \end{aligned} \tag{11}$$

Equation (11) shows that, for the pure irrotational component $\boldsymbol{v_I}$, only its boundary value has contribution to the longitudinal line integral measurements. In other words, inside the sensing area, $\boldsymbol{v_I}$ is invisible to measurements, thus cannot be recovered.

The 2D horizontal velocity field can be considered as a divergence-free vector field [22], which can be uniquely reconstructed from the TOF measurements. This assumption is valid as the stratification in the atmosphere caused by gravity, which makes the horizontal velocity $\boldsymbol{v_{xy}}$ greater than the vertical velocity $\boldsymbol{v_z}$ by a factor of 10–100. Usually for the time-averaged data used here, $\boldsymbol{v_z}$ can be ignored and therefore $\boldsymbol{v_{xy}}$ is considered as a divergence-free vector field and the reconstruction of wind velocity field will not be affected by the invisible field problem.

$$\nabla \cdot \boldsymbol{v_{xy}} = \frac{\partial \boldsymbol{v_x}}{\partial \mathrm{x}} + \frac{\partial \boldsymbol{v_y}}{\partial \mathrm{y}} = -\frac{\partial \boldsymbol{v_z}}{\partial \mathrm{z}} = 0 \tag{12}$$

Among the two divergence-free vector components, v_S and v_H, of the horizontal wind velocity field, it has been proven that, without any other information, both of them can be uniquely recovered from their longitudinal integral measurements [22].

As mentioned before, the forward model describing the relationship between line integral measurements and wind velocity is defined as follow:

$$\boldsymbol{L}_{\boldsymbol{\Gamma}} = \boldsymbol{SV} \tag{13}$$

The inverse problem for the velocity reconstruction has the general form:

$$\min_{V} \|\boldsymbol{L}_{\boldsymbol{\Gamma}} - \boldsymbol{SV}\|_2^2 + \eta\|\boldsymbol{DV}\|_2^2 + \alpha\|\boldsymbol{RV}\|_2^2 \tag{14}$$

where the first term $\|\boldsymbol{L}_{\boldsymbol{\Gamma}} - \boldsymbol{SV}\|_2^2$ is the data fitting term, the second term $\eta\|\boldsymbol{DV}\|_2^2$ is the vector smoothness constraint and $\boldsymbol{D} = \left[\boldsymbol{D}_{\boldsymbol{x}}, \boldsymbol{D}_{\boldsymbol{y}}\right]$ is the divergence operator. $\boldsymbol{D}_{\boldsymbol{x}}, \boldsymbol{D}_{\boldsymbol{y}} \in \mathbb{R}^{N*N}$ are the two directional discrete differentials, which apply discrete 2nd order differential inside the sensing area and 1st order differential for boundary pixel; the third term $\alpha\|\boldsymbol{RV}\|_2^2$ is the vector smoothness constraints, and $\boldsymbol{R}$ is the vector Laplace operator $\boldsymbol{R}V = \nabla^2\boldsymbol{v}$, which can be built using $\boldsymbol{D}_{\boldsymbol{x}}, \boldsymbol{D}_{\boldsymbol{y}}$. Details are showed as below:

$$\begin{aligned} \boldsymbol{RV} = \nabla^2\boldsymbol{v} &= \left(\nabla^2\boldsymbol{v}_{\boldsymbol{x}}, \nabla^2\boldsymbol{v}_{\boldsymbol{y}}\right) \\ &= \left(\frac{\partial^2\boldsymbol{v}_{\boldsymbol{x}}}{\partial x^2} + \frac{\partial^2\boldsymbol{v}_{\boldsymbol{x}}}{\partial y^2}, \frac{\partial^2\boldsymbol{v}_{\boldsymbol{y}}}{\partial x^2} + \frac{\partial^2\boldsymbol{v}_{\boldsymbol{y}}}{\partial y^2}\right) \\ &= \left(\left(\partial_{\boldsymbol{xx}}^2 + \partial_{\boldsymbol{yy}}^2\right)\boldsymbol{v}_{\boldsymbol{x}}, \left(\partial_{\boldsymbol{xx}}^2 + \partial_{\boldsymbol{yy}}^2\right)\boldsymbol{v}_{\boldsymbol{y}}\right) \\ &= \left[\boldsymbol{D}_{\boldsymbol{x}}\boldsymbol{D}_{\boldsymbol{x}} + \boldsymbol{D}_{\boldsymbol{y}}\boldsymbol{D}_{\boldsymbol{y}}, \boldsymbol{D}_{\boldsymbol{x}}\boldsymbol{D}_{\boldsymbol{x}} + \boldsymbol{D}_{\boldsymbol{y}}\boldsymbol{D}_{\boldsymbol{y}}\right]\boldsymbol{V} \end{aligned} \tag{15}$$

Therefore $\boldsymbol{R} = \left[\boldsymbol{D}_{\boldsymbol{x}}\boldsymbol{D}_{\boldsymbol{x}} + \boldsymbol{D}_{\boldsymbol{y}}\boldsymbol{D}_{\boldsymbol{y}}, \boldsymbol{D}_{\boldsymbol{x}}\boldsymbol{D}_{\boldsymbol{x}} + \boldsymbol{D}_{\boldsymbol{y}}\boldsymbol{D}_{\boldsymbol{y}}\right]$.

To solve the inverse problem defined by Eq. (15), an upgrade of Simultaneous Iterative Reconstruction Technique (SIRT) algorithm is applied [9]. This algorithm has the advantage of fast convergence and stability. Generally, it is defined as follow:

$$\boldsymbol{V}^{(\boldsymbol{k}+1)} = \boldsymbol{V}^{(\boldsymbol{k})} + \lambda\boldsymbol{P}\left[\boldsymbol{S}^{\boldsymbol{T}}\boldsymbol{W}\left(L_{\Gamma} - \boldsymbol{S}\boldsymbol{V}^{(\boldsymbol{k})}\right) - \alpha\boldsymbol{R}^{\boldsymbol{T}}\boldsymbol{R}\boldsymbol{V}^{(\boldsymbol{k})} - \eta\boldsymbol{D}^{\boldsymbol{T}}\boldsymbol{D}\boldsymbol{V}^{(\boldsymbol{k})}\right] \tag{16}$$

$$\boldsymbol{P} = \mathrm{diag}(1/LP_1, 1/LP_2, \ldots, 1/LP_{2N}) \tag{17}$$

$$\boldsymbol{W} = \mathrm{diag}(1/LR_1, 1/LR_2, \ldots, 1/LR_{2M}) \tag{18}$$

where λ is the constant iteration step size, α and η are the regularization parameters, k in this section denotes the iteration for linear reconstruction, $LP_j = \sum_{i=1}^{2M} s_{i,j}$ is the directional segment length for all the ray paths across j-th pixel and $\boldsymbol{P}$ is the diagonal preconditioner which is used to geometrically weight the least square cost function and therefore ensure a better noise tolerance and prevent semi-convergence for reconstruction. $LR_i = \sum_{j=1}^{2N} s_{i,j}$ is the length of i-th ray path and $\boldsymbol{W}$ is the normalised operator to make sure that the sum of each row of S equals to 1. By weighting with $\boldsymbol{W}$, when residual norm is minimised, the rays that intersect larger

portions of image can tolerate larger errors than these are much shorter [23]. The iteration step size, λ is chosen so that convergence condition holds

$$0 < \varepsilon < \lambda < \rho \tag{19}$$

where ρ is the matrix radius of $(\boldsymbol{PS^TWS} + \boldsymbol{P}(\boldsymbol{R^TR} + \boldsymbol{D^TD}))$.

In most real-time monitoring system, non-iterative methods are preferred for fast reconstruction speed. To improve the accuracy of non-iterative method, many researchers tried to iteratively calculate the optimal inversion operator beforehand for non-iterative online reconstruction, for instance, Offline Iteration Online Reconstruction (OIOR) [24] based on Landweber iteration, and Direct Landweber (DLW) based on modified Landweber [25]. In order to build a real-time acoustic tomography system, the offline iteration method is applied based on the SIRT method and consequently, the reconstruction time can be reduced to the same level as non-iterative method.

The principle of this method is to design an iteration method, whose iteration procedure is linear and independent of measurement data, which means that the iteration of Eq. (16) can be rewritten as

$$\boldsymbol{V}^{(\boldsymbol{k}+\boldsymbol{1})} = \boldsymbol{BV}^{(\boldsymbol{k})} + \boldsymbol{GL}_{\Gamma} \tag{20}$$

where $\mathbf{B} = \left(\boldsymbol{I} - \boldsymbol{\lambda PS^TWS} - \boldsymbol{\lambda\alpha R^TR} - \boldsymbol{\lambda\eta D^TD}\right)$ and $\mathbf{G} = \boldsymbol{\lambda PS^TW}$

The solution $\boldsymbol{V}^{\boldsymbol{k}+\boldsymbol{1}}$ is decomposed into two parts, the iterative term $\boldsymbol{C}^{\boldsymbol{k}+\boldsymbol{1}}$ and the non-iterative term $\boldsymbol{\varepsilon}$

$$\boldsymbol{V}^{\boldsymbol{k}+\boldsymbol{1}} = \boldsymbol{C}^{\boldsymbol{k}+\boldsymbol{1}}\boldsymbol{\varepsilon} \tag{21}$$

Substituting Eq. (21) into Eq. (20)

$$\boldsymbol{C}^{k+1}\boldsymbol{\varepsilon} = \boldsymbol{BC}^{k}\boldsymbol{\varepsilon} + \boldsymbol{G}L_{\Gamma} \tag{22}$$

Let $\boldsymbol{\varepsilon} = \boldsymbol{L}_{\Gamma}$, then the iterative term $\boldsymbol{C}^{\boldsymbol{k}+\boldsymbol{1}}$ is independent of TOF measurement $\boldsymbol{\tau}$ and can be calculated offline in advance using equation below.

$$\boldsymbol{C}^{k+1} = \boldsymbol{BC}^{k} + \boldsymbol{G} \tag{23}$$

Given the iteration number k, after $\boldsymbol{C}$ is iteratively obtained offline and all the measurements L_{Γ} are measured, the wind velocity $\boldsymbol{V}$ can be determined by Eq. (24).

$$\boldsymbol{V} = \boldsymbol{CL}_{\boldsymbol{\Gamma}} \tag{24}$$

For the offline iteration calculation of $\boldsymbol{C}$, its iteration number k need to be determined beforehand.

3 Simulation Results and Discussions

3.1 TOF Measurement

For the purpose of real-time measurement, the acoustic signal waveform is designed based on the modulated and filtered Kasami sequence. Table 1 illustrates the parameters of generating the waveform for the acoustic source signal. Cross-correlation detection is used to estimate the TOF. In the simulation, all the transmitted signals reached the receivers with preset delay. The cross-correlation detection of TOFs is shown in the Fig. 5, where the arrival time of the transmitted signal from the transceiver 1 to the transceiver 3, 5, 7 and 9 are indicated on the cross-correlation peaks. The overlaps between preset delay and detected delay demonstrate very good accuracy of TOF detection.

Generally, compared with the pairwise TOF measurement process, the total measurement time per frame is reduced from 16 to 1 s.

3.2 Wind Velocity Reconstruction

The performance of proposed vector field reconstruction algorithm is tested on three typical vector field phantoms, including a pure solenoidal vector field $\boldsymbol{v_S}$, a divergence-free vector field which contains the harmonic component $\boldsymbol{v_S} + \boldsymbol{v_H}$, and a composite $\boldsymbol{v_S} + \boldsymbol{v_H} + \boldsymbol{v_I}$ vector field. The last one contains the irrotational vector component when the vertical wind velocity cannot be ignored, despite it is much smaller than the solenoidal component by a factor of 10. To create these phantoms, three fundamental velocity components, solenoidal component $\boldsymbol{v}_S$, irrotational component $\boldsymbol{v_I}$ and harmonic component $\boldsymbol{v_H}$ are created in Fig. 6.

In the simulation, all the TOF measurements contain white Gaussian noise with 40 dB SNR. The algorithm parameters, such as the weight parameter α and η for the divergence-free regularization and vector Laplacian regularization, are empirically determined based on a series of practices and the same parameters are applied

Table 1 Parameters of acoustic waveform

Sampling frequency	200 kHz
Carrier frequency	20 kHz
Band-pass filter bandwidth	10 kHz
Filter length	81
Filter window	Kaiser
Total measurement time per frame	1 s
Pulse duration	0.01 s
Kasami code polynomial	[14, 13, 8, 4, 0]

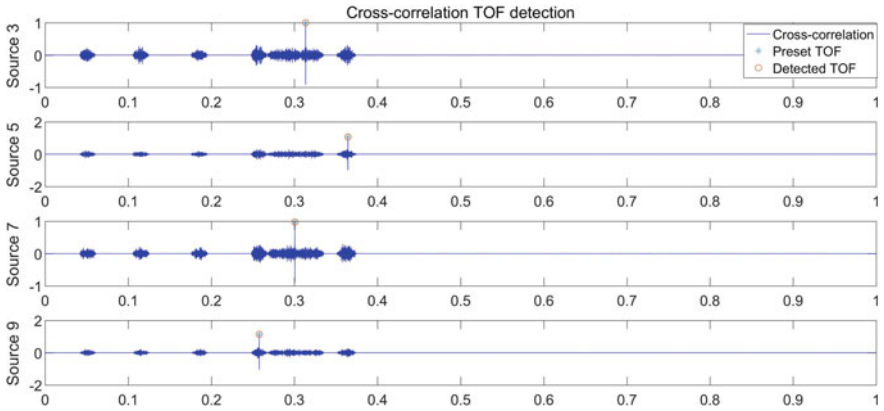

Fig. 5 Cross-correlation TOF detection results from simulation. The preset delay is marked in green asterisks and the detected delay is marked in the red circles (Color figure online)

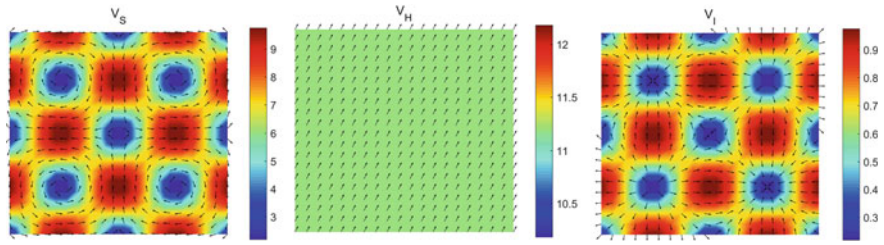

Fig. 6 Three vector field components, from left to right, the solenoidal vector field v_s, the harmonic vector field v_H and the irrotational vector field v_I

to the test phantoms, which is 0.01 and 0.0001 respectively. When implementing the offline iteration algorithm, the pre-calculation iteration number is set to be 200 and the iteration step size is 0.4, which is sufficient for convergence at 40 dB SNR and regularization condition.

To quantitatively evaluate the accuracy of the reconstructed vector field, the relative image error between the reconstructed wind velocity and the true phantom is employed, which is defined as follow:

$$E_{image} = \frac{\|\boldsymbol{V_{re}}(i) - \boldsymbol{V_{ori}}(i)\|_2^2}{\|\boldsymbol{V_{ori}}(i)\|_2^2} \tag{25}$$

Figure 7 illustrates the wind velocity reconstruction results and the relative image errors. The first phantom is designed to evaluate the reconstruction accuracy on the pure solenoidal vector field, where the velocity vanishes at the boundary.

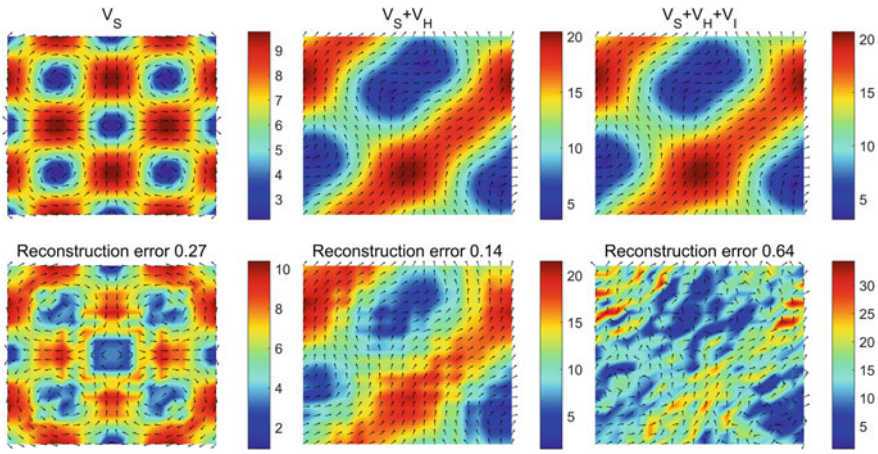

Fig. 7 Simulation phantoms and reconstructed wind velocity fields. The arrows represent the directions of the wind field and the colours indicate its amplitude (Color figure online)

The reconstruction result correctly shows the vortex shape and center positions. There seems to appear some artefact and small discontinuities on the magnitude of the velocity field. The relative image reconstruction error is 0.26, which might be related to the modelling error due to the discretization of the domain and the limited measurement rays paths (96 ray path for 16 transceivers).

The second phantom is designed to evaluate the reconstruction accuracy for the source-free vector field with non-zero boundary velocity, which is a more general case. The velocity field contains the harmonic components, which is both source-free and curl-free, and curl-free means that it also has an invisible field problem. Norton has concluded that measurements of the normal velocity on the boundary can be used to resolve the ambiguity of the harmonic part, and then v_S and v_H can be recovered separately [21]. Later, Ivana further proved that no extra measurements are needed to determine the source-free vector field $v_S + v_H$. Because the entire vector field needs to be reconstructed, it is not necessary to sperate two components [22]. The relative reconstruction error of the second phantom is 0.14, which is lower than the error of the first case. This is due to the low complexity of harmonic component.

The third phantom tests the velocity field when the irrotational component cannot be ignored. The relative image error increases to 0.64 in this case. The reconstruction accuracy is largely affected by the irrotational component, even the source-free component is much larger than the irrotational vector field by a factor of 10. This phantom shows that acoustic travel-time tomography is more suitable for the horizontal slice of wind velocity in the stratified atmosphere, where the wind velocity is a 2D source-free vector field.

4 Conclusion

In this chapter, the fundamental methods of acoustic tomography system are studied for wind velocity field measurement, including the simultaneous acoustics signal transmission and time-of-flight (TOF) collection along multiple ray paths, and offline iteration vector field reconstruction algorithm. In this mode of operation, TOF detection process for different paths is performed simultaneously based on cross-correlation detection. For wind velocity field reconstruction, iterative reconstruction with the divergence-free and vector Laplacian regularization is applied in an offline mode for online reconstruction with good quantitative accuracy. Three different wind velocity fields are simulated to evaluate the performance of the reconstruction method. The results of feasibility study show that acoustic tomography can provide tomographic images of the wind velocity field in a relatively good accuracy.

References

1. Marchigiani R et al (2013) Wind disasters: a comprehensive review of current management strategies. Int J Crit Illn Inj Sci 3(2):130–142
2. Tamura Y (2009) Wind induced damage to buildings and disaster risk reduction. In: Proceedings of the APCWE-VII, Taipei, Taiwan
3. Mikkelsen T (2010) Remote sensing of wind. Remote sensing for wind energy, pp 7–20
4. Sheh R et al (2006) A low-cost, compact, lightweight 3d range sensor. In: Australian conference on robotics and automation
5. Spiesberger JL, Fristrup KM (1990) Passive localization of calling animals and sensing of their acoustic environment using acoustic tomography. Am Nat 135:107–153
6. Keith Wilson D, Thomson DW (1994) Acoustic tomographic monitoring of the atmospheric surface layer. J Atmos Oceanic Technol 11(3):751–769
7. Vecherin SN et al (2007) Tomographic reconstruction of atmospheric turbulence with the use of time-dependent stochastic inversion. J Acoust Soc Am 122(3):1416–1425
8. Ziemann A, Arnold K, Raabe A (2002) Acoustic tomography as a remote sensing method to investigate the near-surface atmospheric boundary layer in comparison with in situ measurements. J Atmos Oceanic Technol 19(8):1208–1215
9. Ziemann A, Arnold K, Raabe A (1998) Acoustic tomography in the atmospheric surface layer. In: Annales Geophysicae. Springer, Berlin
10. Ostashev V et al (2008) Recent progress in acoustic tomography of the atmosphere. In: IOP conference series: earth and environmental science. IOP Publishing
11. Holstein P et al (2004) Acoustic tomography on the basis of travel-time measurement. Meas Sci Technol 15(7):1420
12. Jovanovic I (2008) Inverse problems in acoustic tomography
13. Jovanovic I et al (2007) Efficient and stable acoustic tomography using sparse reconstruction methods. In: 19th international congress on acoustics
14. Dogan Z et al (2012) 3D reconstruction of wave-propagated point sources from boundary measurements using joint sparsity and finite rate of innovation. In: 2012 9th IEEE international symposium on biomedical imaging (ISBI). IEEE
15. Toši I et al (2010) Ultrasound tomography with learned dictionaries. In: 2010 IEEE international conference on acoustics, speech and signal processing. IEEE

16. Vecherin SN et al (2006) Time-dependent stochastic inversion in acoustic travel-time tomography of the atmosphere. J Acoust Soc Am 119(5):2579–2588
17. Liu Y et al (2015) A method for simultaneous reconstruction of temperature and concentration distribution in gas mixtures based on acoustic tomography. Acoust Phys 61(5):597–605
18. Kolouri S, Azimi-Sadjadi MR, Ziemann A (2014) Acoustic tomography of the atmosphere using unscented Kalman filter. IEEE Trans Geosci Remote Sens 52(4):2159–2171
19. Ostashev VE, Wilson DK (2015) Acoustics in moving inhomogeneous media. CRC Press, Boca Raton
20. Li H, Takata S, Yamada A (2011) Tomographic measurement of vortex air flow field using multichannel transmission and reception of coded acoustic wave signals. Jpn J Appl Phys 50 (7S):07HC09
21. Norton SJ (1992) Unique tomographic reconstruction of vector fields using boundary data. IEEE Trans Image Process 1(3):406–412
22. Jovanovic I, Sbaiz L, Vetterli M (2009) Acoustic tomography for scalar and vector fields: theory and application to temperature and wind estimation. J Atmos Oceanic Technol 26 (8):1475–1492
23. Gregor J, Fessler JA (2015) Comparison of SIRT and SQS for regularized weighted least squares image reconstruction. IEEE Trans Comput Imaging 1(1):44–55
24. Liu S et al (2004) Prior-online iteration for image reconstruction with electrical capacitance tomography. IEE Proc Sci Meas Technol 151(3):195–200
25. Kim BS et al (2015) Electrical resistance imaging of two-phase flow using direct Landweber method. Flow Meas Instrum 41:41–49